COL4A1 Mutations Cause Neuromuscular Disease with Tissue-Specific Mechanistic Heterogeneity

Cassandre Labelle-Dumais,[1] Vera Schuitema,[1] Genki Hayashi,[1] Kendall Hoff,[1] Wenhui Gong,[2] Dang Q. Dao,[1] Erik M. Ullian,[1] Peter Oishi,[2] Marta Margeta,[3] and Douglas B. Gould[1,4,5,*]

Collagen type IV alpha 1 and alpha 2 chains form heterotrimers ($[\alpha1(IV)]_2\alpha2(IV)$) that represent a fundamental basement membrane constituent. Dominant *COL4A1* and *COL4A2* mutations cause a multisystem disorder that is marked by clinical heterogeneity and variable expressivity and that is generally characterized by the presence of cerebrovascular disease with ocular, renal, and muscular involvement. Despite the fact that muscle pathology is reported in up to one-third of individuals with *COL4A1* and *COL4A2* mutations and in animal models with mutations in *COL4A1* and *COL4A2* orthologs, the pathophysiological mechanisms underlying *COL4A1*-related myopathy are unknown. In general, mutations are thought to impair $[\alpha1(IV)]_2\alpha2(IV)$ secretion. Whether pathogenesis results from intracellular retention, extracellular deficiency, or the presence of mutant proteins in basement membranes represents an important gap in knowledge and a major obstacle for developing targeted interventions. We report that *Col4a1* mutant mice develop progressive neuromuscular pathology that models human disease. We demonstrate that independent muscular, neural, and vascular insults contribute to neuromyopathy and that there is mechanistic heterogeneity among tissues. Importantly, we provide evidence of a COL4A1 functional subdomain with disproportionate significance for tissue-specific pathology and demonstrate that a potential therapeutic strategy aimed at promoting $[\alpha1(IV)]_2\alpha2(IV)$ secretion can ameliorate or exacerbate myopathy in a mutation-dependent manner. These data have important translational implications for prediction of clinical outcomes based on genotype, development of mechanism-based interventions, and genetic stratification for clinical trials. Collectively, our data underscore the importance of the $[\alpha1(IV)]2\alpha2(IV)$ network as a multifunctional signaling platform and show that allelic and tissue-specific mechanistic heterogeneities contribute to the variable expressivity of *COL4A1* and *COL4A2* mutations.

Introduction

Mutations in genes coding for collagen type IV alpha 1 (COL4A1) and alpha 2 (COL4A2) chains cause a multisystem disorder that is generally characterized by the presence of cerebrovascular disease with variable ocular, renal, and muscular involvement (MIM: 607595, 614519, 175780).[1–3] Athough most studies have focused on cerebrovascular manifestations, many aspects of the COL4A1/A2 syndrome are still emerging and remain understudied. For instance, despite the fact that muscle pathology has been reported in up to one-third of individuals with *COL4A1* (MIM: 120130) and *COL4A2* (MIM: 120090) mutations[1] and in animal models (mice, *C. elegans,* and *Drosophila*) with mutations in *COL4A1* and *COL4A2* orthologs,[4–9] virtually nothing is known about the pathogenic mechanisms underlying COL4A1- and COL4A2-related myopathy. Mice that carry a *Col4a1* splice-site mutation leading to skipping of exon 41 ($Col4a1^{\Delta ex41}$)[10,11] have transient neuromuscular-junction abnormalities during the early postnatal period[12] and develop genetically complex skeletal myopathy characterized by reduced grip strength, elevated serum creatine kinase (CK) concentrations, and increased numbers of non-peripheral nuclei (NPN).[4,5] $Col4a1^{+/\Delta ex41}$ mice also have ocular dysgenesis and cerebral cortical lamination defects that are characteristic of dystroglycanopathies such as muscle-eye-brain disease and Walker-Warburg syndrome (MIM: 253280, 236670), suggesting that there might be shared pathophysiology between dystroglycan deficiency and COL4A1/A2 syndrome.[5]

COL4A1 and *COL4A2* arose ~750 million years ago with the emergence of multicellular organisms[13,14] and produce heterotrimers ($[\alpha1(IV)]_2\alpha2(IV)$) that are ubiquitously present during development and in nearly all mature basement membranes (BMs).[13] Despite this broad distribution, remarkable conservation, and the vast clinical spectrum of human diseases resulting from *COL4A1* and *COL4A2* mutations, the biological functions of $[\alpha1(IV)]_2\alpha2(IV)$ are poorly defined. The COL4A1 and COL4A2 proteins each consist of three domains; a large triple-helical domain and the flanking 7S and non-collagenous (NC1) domains at the amino and carboxy termini, respectively. Within the endoplasmic reticulum (ER), the NC1 domains initiate heterotrimer assembly, which proceeds by the progressive winding of the triple-helical domains. The pathogenicity of *COL4A1* and *COL4A2* mutations is generally attributed to misfolding and impaired secretion of mutant $[\alpha1(IV)]_2\alpha2(IV)$, and both intracellular retention and extracellular deficiency of $[\alpha1(IV)]_2\alpha2(IV)$ have been proposed as important pathogenic events. Using a chemical chaperone to promote $[\alpha1(IV)]_2\alpha2(IV)$ secretion

[1]Department of Ophthalmology, University of California, San Francisco, San Francisco, CA 94143, USA; [2]Department of Pediatrics, University of California, San Francisco, San Francisco, CA 94143, USA; [3]Department of Pathology, University of California, San Francisco, San Francisco, CA 94143, USA; [4]Department of Anatomy, University of California, San Francisco, San Francisco, CA 94143, USA; [5]Institute for Human Genetics, University of California, San Francisco, San Francisco, CA 94143, USA
*Correspondence: douglas.gould@ucsf.edu
https://doi.org/10.1016/j.ajhg.2019.03.007.

reduced intracerebral hemorrhages (ICHs) in *Col4a1*$^{+/\Delta ex41}$ mice.[15,16] However, because chemical chaperones simultaneously decrease intracellular and increase extracellular [α1(IV)]$_2$α2(IV) levels, the issue of whether pathology is caused by intracellular accumulation or extracellular deficiency remains unresolved. Moreover, the possibility that the presence of mutant [α1(IV)]$_2$α2(IV) in the BM could also contribute to pathology[17] has never been addressed and could have important implications for the development of targeted therapeutic interventions for individuals with *COL4A1* and *COL4A2* mutations. Conceptually, and in light of our recent findings, pharmacologically promoting [α1(IV)]$_2$α2(IV) secretion might be beneficial for individuals with *COL4A1* and *COL4A2* mutations. However, if the presence of mutant [α1(IV)]$_2$α2(IV) in BMs is pathogenic (via disruption of BM structure, altered cell-matrix adhesion, perturbation of downstream signaling, etc.), it is conceivable that promoting the secretion of mutant [α1(IV)]$_2$α2(IV) could induce or exacerbate pathology in some tissues in a mutation-dependent manner. Thus, a fundamental question for understanding COL4A1- and COL4A2-related diseases is whether pathogenesis results from a primary intracellular or extracellular insult and, if extracellular, whether it is caused by [α1(IV)]$_2$α2(IV) deficiency or by the presence of mutant proteins in the BM.

Using an allelic series of nine different murine *Col4a1* and *Col4a2* mutations, we identified a position-dependent effect on heterotrimer biosynthesis that correlated with ICH severity. We found that mutations closer to the carboxy terminus of the triple-helical domain caused greater intracellular accumulation and more severe ICHs.[4,18,19] In contrast, there was no clear correlation between secretion efficiency and myopathy severity. Instead, the mutation nearest the amino terminus of the COL4A1 protein (*Col4a1*^{G394V}), which was among the mutations with the least intracellular accumulation and mildest ICHs, caused the most severe myopathy.[1,2,4] This observation supports the notion that the presence of mutant [α1(IV)]$_2$α2(IV) in BMs can contribute to pathology in a tissue-specific manner and suggests that mutations affecting specific functional subdomains differentially contribute to distinct aspects of the COL4A1/A2 syndrome.

In this study, we describe myopathic changes in skeletal muscles from an individual with a *COL4A1* mutation. In addition, we use a combination of histological, biochemical, functional, and genetic approaches to perform a detailed characterization of COL4A1-related neuromyopathy in two *Col4a1* mutant mouse strains with distinct properties. We show that *Col4a1* mutant mice develop progressive skeletal myopathy that models pathology observed in individuals with *COL4A1* mutations, identify a role for COL4A1 in peripheral myelination, and use conditional gene targeting to demonstrate a vascular contribution to COL4A1-related myopathy. Importantly, we identify mutation-dependent and tissue-specific responses to a potential therapeutic strategy. Understanding genotype-dependent responses to therapeutic agents is critical for effective design of clinical trials and for developing personalized interventional strategies, both of which have significant implications for individuals with *COL4A1* and *COL4A2* mutations.

Material and Methods

Pathologic Evaluation

Clinical and pathology reports were obtained from the University of California, San Francisco (UCSF) electronic medical records; the permission to use tissue for research was covered by the autopsy permit signed by the individual's next-of-kin. No individually identifiable data are presented in this report. Iliopsoas samples were taken during autopsy and processed for formalin-fixed, paraffin-embedded sections (UCSF Clinical Histology Laboratory) and frozen sections (UCSF Laboratory for Neuromuscular Special Studies). Paraffin sections were evaluated by hematoxylin and eosin (H&E) staining, and the flash-frozen muscle was evaluated with a standard panel of muscle stains (H&E; modified trichrome; ATPase [pH 9.4]; reduced NADH-tetrazolium reductase [NADH-TR]; succinic dehydrogenase [SDH]; cytochrome oxidase [COX]; combined COX-SDH; and dual immunohistochemistry for slow and fast myosin proteins). The slides were scanned with the Aperio whole-slide scanner, and relevant microscopic fields were extracted with Aperio ImageScope software (both from Leica Biosystems); the final images were edited with Adobe Photoshop.

Animals

All experiments were conducted in compliance with protocols approved by the Institutional Animal Care and Use Committee at UCSF (protocols AN102193 and AN159737). The two *Col4a1* mutant mouse lines (*Col4a1*$^{+/\Delta ex41}$ and *Col4a1*$^{+/G394V}$) were described previously.[4,11,19] (Note: The *Col4a1*$^{\Delta ex41}$ mutation was originally reported as *Col4a1*$^{\Delta ex40}$ but has been updated to reflect subsequent genome annotations.[3]) All mutant mice used in this study were heterozygous for a given *Col4a1* mutation that was iteratively crossed to C57BL/6J (B6) mice for a minimum of 12 generations. Both male and female mice were used in all experiments and, except for an expected difference in body weight, no differences were observed between sexes, and no samples were excluded from the study. The conditional *Col4a1*^{Flex41} mutant mouse was generated by InGenious Targeting Laboratory and previously characterized.[16,20] The ubiquitous *Actb*^{Cre} line[21] was used for validation of the conditional *Col4a1*^{Flex41} allele. The *Tek-Cre* line[22] was used for induction of endothelial-cell-specific expression of the conditional *Col4a1*^{Flex41} allele.

In Vivo Procedures

Grip-Strength Measurements

Peak grip force was determined with a grip-strength meter (AMETEK TCI Division Chatillon Force Measurement Systems; re-sold by Columbus Instruments); the average from three consecutive trials was used for each animal. In brief, the grip-strength meter consists of a bar (forelimb) or a grid (forelimb and hindlimb) connected to a force meter. We tested grip strength by holding the mouse over a bar or grid until the mouse gripped the steel bars; then the mouse was pulled away from the force meter until it released the bar or grid.

4PBA Treatment

Sodium 4-phenylbutyrate (4PBA; Scandinavian Formulas) was provided in drinking water and refreshed weekly. Embryonic day (E) 9.5 was chosen as a starting point for treatment to avoid potential implantation perturbations and minimize possible teratogenic effects. The day of fertilization (E0.5) was assessed by the presence of vaginal plug.

Serum CK Enzyme Assay

Blood was drawn from the submandibular vein, and serum was collected with microtainer serum separator tubes (BD, catalog #365956). CK enzyme activities were measured with a CK reagent kit (Pointe Scientific; catalog #C7512-39) and microplate reader (VersaMax, Molecular Devices) according to the manufacturer's instructions.

Ex Vivo Procedures

Myo-Mechanical Analysis of Isolated Skeletal Muscles

Maximal twitch and tetanic tensions were determined as described previously.[23,24] In brief, extensor digitorum longus muscles were gently harvested under a dissection microscope in the presence of buffered lactated Ringer's solution to mimic physiological conditions. The muscles were isolated so that as much tendon as possible could be preserved at each end and were transferred into a Petri dish containing Ringer's solution. We used sutures to tie each of the muscle tendons and avoided contact with muscle fibers. Isolated muscles were mounted in an integrated muscle-strip myograph bath (from Danish Myo Technology, DMT Model 820MS) in physiological solution at constant temperature with continuous oxygenation (Krebs Henseleit solution, 25°C, oxygenated with O_2/CO_2 [95%/5%]). Myo-mechanical responses were measured with a square-pulse electrical stimulator (Grass Model S48) and a data acquisition platform (AD Instruments PowerLab Data Acquisition System and LabChart software).

Peripheral Nerve Conduction Velocities

Conduction action potential (CAP) recordings were performed as previously described.[25] In brief, sciatic nerves were isolated from mice under anesthesia and transferred to oxygenated recording solution (125 mM NaCl, 2.5 mM KCl, 1 mM $MgCl_2$, 2 mM $CaCl_2$, 10 mM D-glucose, 1.25 mM NaH_2PO_4, and 25 mM $NaHCO_3$). We measured CAPs,under perfusion of recording solution, with suction electrodes at room temperature by stimulating the nerve from one end and recording at the other end. Signals were acquired with a differential AC amplifier (model 1700, AM Systems) and digitized (Axon Digidata 1440A, Molecular Devices). Constant current stimulation (50 μs) was delivered to the stimulus electrode with a stimulus isolator (ISO-Flex, A.M.P.I.). Oxygenated recording solution was perfused by gravity into the recording chamber and removed via a peristaltic pump. We measured CAPs at room temperature by delivering current via the stimulus electrode on one end of the nerve while recording the voltage response at the other end. We determined conductance velocity by dividing the length of the nerve by the latency between the start of the stimulus artifact and the peak of the CAP.

Histological and Molecular Analyses

Muscle Histopathology and Quantification of NPN

Mice in the 2-month-old cohorts were challenged with exercise after grip-strength and serum-CK measurements. Each exercise session included a 2 min acclimation period followed by a 30 min exercise challenge involving a 15° downhill grade on a treadmill equipped with a shock plate (Exer 3/6, Columbus Instruments). Animals were started at 7 m/min and increased by 1 m/min each minute until a maximum of speed of 11 m/min was reached. Exercise challenges consisted of five consecutive sessions performed 3 days apart. Immediately after dissection, quadriceps, soleus, tibialis anterior, and triceps were flash frozen in liquid-nitrogen-chilled isopentane. Cryosections (10 μm) were collected from the central portions of the muscles at regular intervals (200 μm) and stained with H&E for histopathological analysis and determination of the numbers of NPN. Between 16 and 20 sections were examined per muscle, and one random field of view (20×) was imaged for each section for subsequent NPN quantification. Histochemical staining for COX activity was performed according to previously published methods.[26] In brief, muscle cryosections were exposed to COX reaction media (4 mM diaminoben, zidine tetrahydrochloride, 100 μM, cytochrome C, and 20 μg/mL catalase in 0.2 M phosphate buffer [pH 7.0]) for 2 h at 37°C, dehydrated, and placed under coverslips applied with Permount.

Electron Microscope Histological Analysis of Peripheral Nerve Myelination

Sciatic nerves were collected from postnatal (P6) and adult (2- to 3-month-old) mice. Adult mice were transcardially perfused with PBS, followed by 1% paraformaldehyde (PFA) prior to nerve collection. Sciatic nerves were immersion fixed in EM fixative (2% PFA and 2.5% glutaraldehyde in 0.1 M phosphate buffer, pH = 7.4) and processed for electron microscopy by the UCSF Veterans Affairs Medical Center Pathology Core. In brief, fixed sciatic nerves were cut transversely into 1.5-mm-thick blocks. Blocks were further fixed in osmium tetroxide overnight at 4°C, dehydrated through ascending ethanol washes, and embedded in resin (TAAB Laboratories). Sections (1 μm) were cut and examined by electron microscopy.

Analyses of g-Ratios

g-ratios were calculated as axon area divided by the area of both the axon and the associated myelin sheath. The images of transverse sciatic nerve sections were acquired at 2,000× magnification. Digitized and calibrated images were used for morphometric analysis with ImageJ (National Institutes of Health).

Immunoblot Analyses

Isolation, culture, and COL4A1 immunoblotting of mouse embryonic fibroblasts (MEFs) was described previously,[4] and rabbit anti-laminin 1 + 2 antibody (1:2,000, ab7463, Abcam) was used as an extracellular loading control. For sciatic-nerve samples, proteins were extracted in radioimmunoprecipitation assay (RIPA) buffer containing 50 mM Tris (pH 8.0), 150 mM NaCl, 2 mM EDTA, 1% NP-40, 0.5% Na deoxycholic acid, and 1 mM 0.1% SDS, supplemented with a complete protease inhibitor cocktail (Pierce, USA) at 4°C. After centrifugation (13,000 rpm, 20 min at 4°C), the soluble fraction was collected. Samples were separated on a 4%–15% gradient SDS-PAGE gel under non-reducing (conditioned medium) or reducing (peripheral nerve lysates) conditions and transferred to polyvinylidene fluoride (PVDF) membranes (Bio-Rad). Membranes were blocked for 1 h at room temperature in 5% non-fat milk in Tris-buffered saline (TBS) containing 0.1% Tween-20 (TBS-T) and incubated overnight at 4°C with rat monoclonal anti-myelin-basic-protein (anti-MBP) antibody (Abcam ab7349, 1:500). Mouse monoclonal anti-γ-tubulin antibody (1:5000, T6557, Sigma) or polyclonal chicken anti-beta actin (1:1000, Ab13822, Abcam) was used as a loading control. After incubation with primary antibodies, membranes were incubated with horseradish peroxidase-conjugated secondary antibodies (donkey anti-rat, -rabbit, or -mouse IgG, 1:10 000, Jackson

ImmunoResearch) diluted in 5% non-fat milk in TBS-T for 1 h at room temperature. Immunoreactivity was visualized by chemiluminescence (Pierce ECL Chemiluminescent Substrate, Thermo Scientific). Densitometric analysis was performed on low-exposure images with ImageJ (National Institutes of Health).

Immunolabeling

Myelin basic protein (MBP) immunolabeling was performed on 20 μm cryosections that were fixed in 4% PFA in PBS, blocked for 1 h at room temperature in blocking buffer (PBS containing 10% normal donkey serum and 0.1% Triton X-100), and incubated overnight at 4°C with or rat anti-MBP (Abcam, ab7349, 1:500) antibodies in blocking buffer. Immunolabeling was visualized with AlexaFluor-594-conjugated secondary antibodies (raised in donkey, 1:500, Invitrogen-Molecular Probes) in blocking buffer. Dual myosin-heavy-chain (MHC) immunolabeling for myofiber typing was performed on 20 μm cryosections from soleus muscles as described previously.[27] In brief, sections were blocked for 1 h at room temperature in PBS containing 10% normal goat serum and incubated overnight at 4°C with a combination of antibodies against type I and type II MHC (BA-F8 [1:50] and SC-71 [1:600]) diluted in blocking buffer. Immunolabeling was visualized with AlexaFluor-594- or -488-conjugated secondary antibodies raised in goat (1:500, Invitrogen Molecular Probes). Slides were mounted with Mowiol containing DAPI (4′, 6-diamidino-2-phenylindole; 2 μg/mL) so that nuclei would be labeled.

Perls' Prussian Blue Staining and Analysis and Quantification of Cerebral Hemorrhage

Quantification of cerebral hemorrhage severity was preformed with Perls' Prussian Blue staining and CellProfiler as described previously.[16]

Microscopy

Images were captured with AxioVision software and an AxioImager M1 microscope equipped with an AxioCam MRm digital camera for fluorescence or an AxioCam ICc3 for bright-field microscopy (Carl Zeiss Microscopy).

Statistical Analyses

For comparisons across genotypes, p values were calculated with Kruskal-Wallis tests with Dunnets pairwise tests (Bonferroni corrected). Effect of age or 4PBA treatment for a given genotype was evaluated with Wilcoxon rank-sum tests. p values <0.05 were considered significant. Data are presented as the median and interquartile range.

Results

Similar Myopathic Changes in Skeletal Muscles from an Individual and Mice with COL4A1/Col4a1 Mutations

We analyzed autopsy skeletal muscle samples from an individual who had a *COL4A1* mutation (c.2317G>A [p.Gly773Arg]) and who died after an episode of cardiac arrhythmia during cataract removal surgery at 10 weeks of age. (Some aspects of this case were previously reported.[28]) The general autopsy revealed acute superimposed on chronic ischemic encephalopathy and hypertrophic cardiomyopathy. Histological examination of iliopsoas autopsy samples revealed randomly distributed, patchy myopathic lesions characterized by myofiber size variation, endomysial fibrosis, and focal fatty replacement (Figures 1A–1A″). Dual immunolabeling for MHCs revealed a relatively normal distribution of type I and type II myofibers (Figures 1B–1B″). Although the initial report raised the possibility of mitochondrial defects,[28] we found that COX-deficient fibers were also negative for succinate dehydrogenase (SDH) activity and were found exclusively in the affected areas, consistent with a nonspecific pattern of muscle-fiber injury (Figures 1C–1C″). Histological analyses of skeletal muscles from *Col4a1* mutant mice revealed a similar spectrum of myopathic changes; these included NPN, variable fiber size, clusters of necrotic and regenerating myofibers, endomysial fibrosis, and secondary infiltration of inflammatory cells (Figures 2A–2F). Consistent with observations in the human muscle biopsy, *Col4a1* mutant mice showed no abnormalities in the distribution of type I and type II fibers (Figures 2G–2I); furthermore, COX staining did not reveal evidence of any mitochondrial defects (Figures 2J–2L). Notably, myopathic lesions observed in *Col4a1* mutant skeletal muscles also had a patchy distribution (often showing perifascicular prominence) and appeared to represent lesions at different stages of the same disease process.

General and Progressive Skeletal Myopathy in *Col4a1*-Mutant Mice

To better define pathology caused by *Col4a1* mutations, we characterized myopathy in two different *Col4a1* mutant mouse strains—$Col4a1^{\Delta ex41}$ and $Col4a1^{G394V}$. We selected these strains from an allelic series of *Col4a1* mutant mice because they showed the most severe myopathy according to NPN quantification in quadriceps while having different effects on $[\alpha1(IV)]_2\alpha2(IV)$ secretion.[4] Both mutations occur in the COL4A1 triple-helical domain; the $Col4a1^{\Delta ex41}$ mutation is a splice acceptor mutation leading to skipping of exon 41 (amino acids 1169–1185), whereas $Col4a1^{G394V}$ is an archetypal glycine missense mutation. Notably, the $Col4a1^{\Delta ex41}$ mutation significantly impairs $[\alpha1(IV)]_2\alpha2(IV)$ secretion, whereas the $Col4a1^{G394V}$ mutation does not[4] (Figure S1). Mutant mice had significantly increased numbers of NPN in all muscle types examined (Figures 3A–3D), and both strains had significantly elevated serum CK concentrations (Figure 3E). In addition, increases in NPN numbers and CK concentrations were more pronounced with age, suggesting that myopathy is progressive.

To test whether the histological and biochemical changes reflected impaired myo-mechanical properties, we analyzed isolated extensor digitorum longus and found significantly reduced maximal tetanic tension in $Col4a1^{+/\Delta ex41}$ and $Col4a1^{+/G394V}$ mice, and there were significantly lower maximal twitch tensions in $Col4a1^{+/G394V}$ mice than in either $Col4a1^{+/+}$ or $Col4a1^{+/\Delta ex41}$ mice (Figures 4A–4C). Together with measures of histological and biochemical outcomes, these observations support the conclusion that myopathy is more severe in $Col4a1^{+/G394V}$ than in $Col4a1^{+/\Delta ex41}$ mice. In contrast, while both $Col4a1^{+/\Delta ex41}$ and $Col4a1^{+/G394V}$ mice had reduced grip forces compared to $Col4a1^{+/+}$ littermates (Figures 4D–4F), grip strength was significantly lower in $Col4a1^{+/\Delta ex41}$ compared to $Col4a1^{+/G394V}$ mice at 2 months. Because grip strength

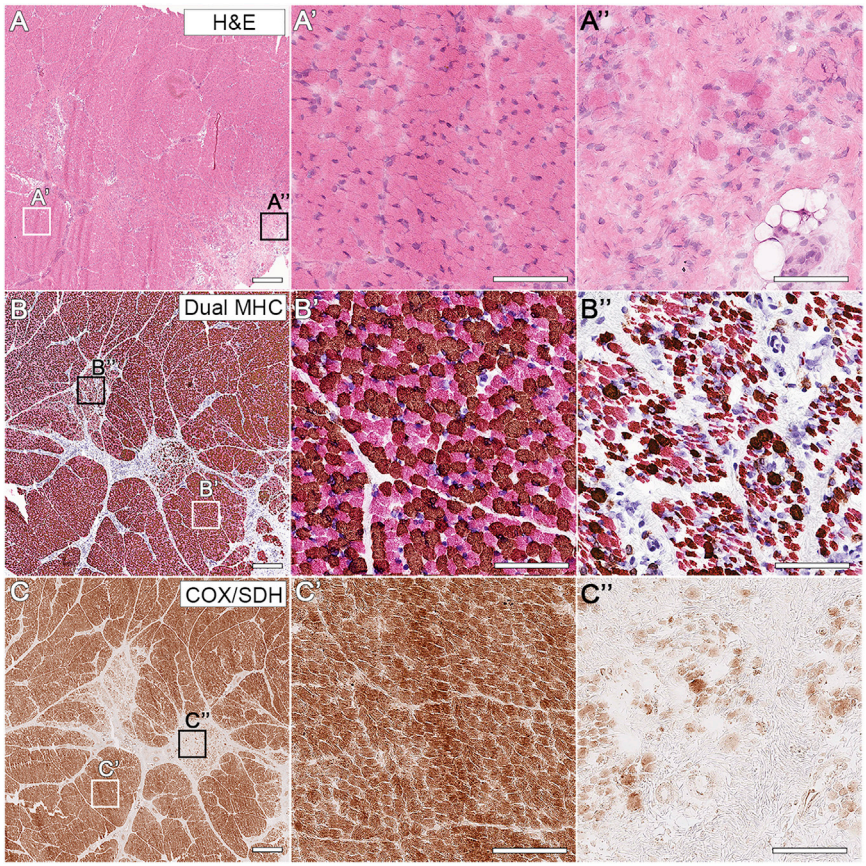

Figure 1. Focal Myopathic Changes in Skeletal Muscles from an Individual with a *COL4A1*^{G773R} Mutation

(A–C″) Skeletal muscle histopathology from a female who had a p.Gly773Arg COL4A1 alteration and who died from surgery complications at 10 weeks of age. Representative images of sections from iliopsoas stained with H&E (A–A″), immunolabeled for MHC type I (brown) and II (pink) (B–B″), and stained for COX/SDH activity (C–C″) highlight the patchy nature of the disease process; affected fascicles are surrounded by unremarkable fascicles (A, B, and C). Unaffected areas from the iliopsoas (A′, B′, and C′, high magnification of white-boxed areas in A, B, and C, respectively) show tightly packed, evenly sized fibers (A′) with characteristic checkerboard distribution of type I and type II myofibers (B′) and normal COX activity (C′). Affected areas from the same muscle (A″, B″, and C″, high magnification of black-boxed areas in A, B, and C, respectively) show marked variation in fiber size; endomysial fibrosis; focal fatty change (A″); normal distribution of type I and type II myofibers (B″); and nonspecific loss of COX acitivity (illustrated by the presence of COX-deficient fibers that also lack SDH activity [C″]).
Scale bars represent 500 μm (A–C); and 100 μm (A′–C′ and A″–C″).

reflects the functional integration of multiple systems, these data suggest that other tissues that are differentially affected by the two mutations might be contributing to COL4A1-related myopathy. Collectively, these findings demonstrate that *Col4a1* mutations cause generalized and progressive skeletal myopathy that is modulated by allelic heterogeneity and potentially involves contributions of extra-muscular tissues.

Col4a1-Mutant Mice Have Hypomyelination of Peripheral Nerves

COL4A1 was recently identified as a ligand for the adhesion G-protein-coupled receptor GPR126, which is required for Schwann cell maturation.[29–31] To begin addressing the potential contribution of extra-muscular tissues to COL4A1-related myopathy, we tested whether *Col4a1*-mutant mice have peripheral nerve abnormalities. We first assessed peripheral nerve myelination by using area-based g-ratios to quantify myelin thickness on electron micrographs of sciatic nerves from 2-to-3-month old mice; we found a small but significant decrease in myelination in *Col4a1*$^{+/\Delta ex41}$ mice (Figure S2). We also detected a significant reduction in myelin thickness in sciatic nerves from *Col4a1*$^{+/\Delta ex41}$ mice at postnatal day 6 (P6) (Figures 5A–5C). Notably, at this age, we observed abnormally large bundles of unmyelinated axons with irregular morphology, mixed-caliber axons, and abnormally thin Schwann cell processes between individual axons, suggestive of impaired radial sorting (Figures 5A, 5B, and 5D). In agreement with these observations, immunoblot analyses and immunolabeling revealed reduced MBP levels in nerves from *Col4a1*$^{+/\Delta ex41}$ mice during the early postnatal period (Figures 5E–5G). Finally, we detected significantly reduced conduction velocities in sciatic nerves from P7 *Col4a1*$^{+/\Delta ex41}$ mice (Figure 5H). Collectively, these ultrastructural, molecular, and physiological data identify developmental peripheral neuropathy in *Col4a1*$^{+/\Delta ex41}$ mice for the first time.

Vascular Abnormalities Contribute to Myopathy in *Col4a1*-Mutant Mice

Col4a1 mutations cause vascular defects in multiple organs, and the prominent perifascicular distribution of myopathic lesions is consistent with a vascular etiology. To directly interrogate the role of vasculature in myopathy caused by *Col4a1* mutations, we used a conditional *Col4a1* mutant allele (*Col4a1*^{Flex41}) that recreates the *Col4a1*$^{\Delta ex41}$ mutation in a Cre-dependent manner.[16,20,32] We first crossed *Col4a1*$^{+/Flex41}$ mice to the ubiquitous *Actb*–Cre line and found that *Col4a1*$^{+/Flex41}$ mice were indistinguishable from *Col4a1*$^{+/+}$ mice and that *Actb*^{Cre};*Col4a1*$^{+/Flex41}$ littermates had significantly increased numbers of NPN and reduced grip strength; these findings were comparable to those observed in *Col4a1*$^{+/\Delta ex41}$ mice (Figures S3A–S3D).

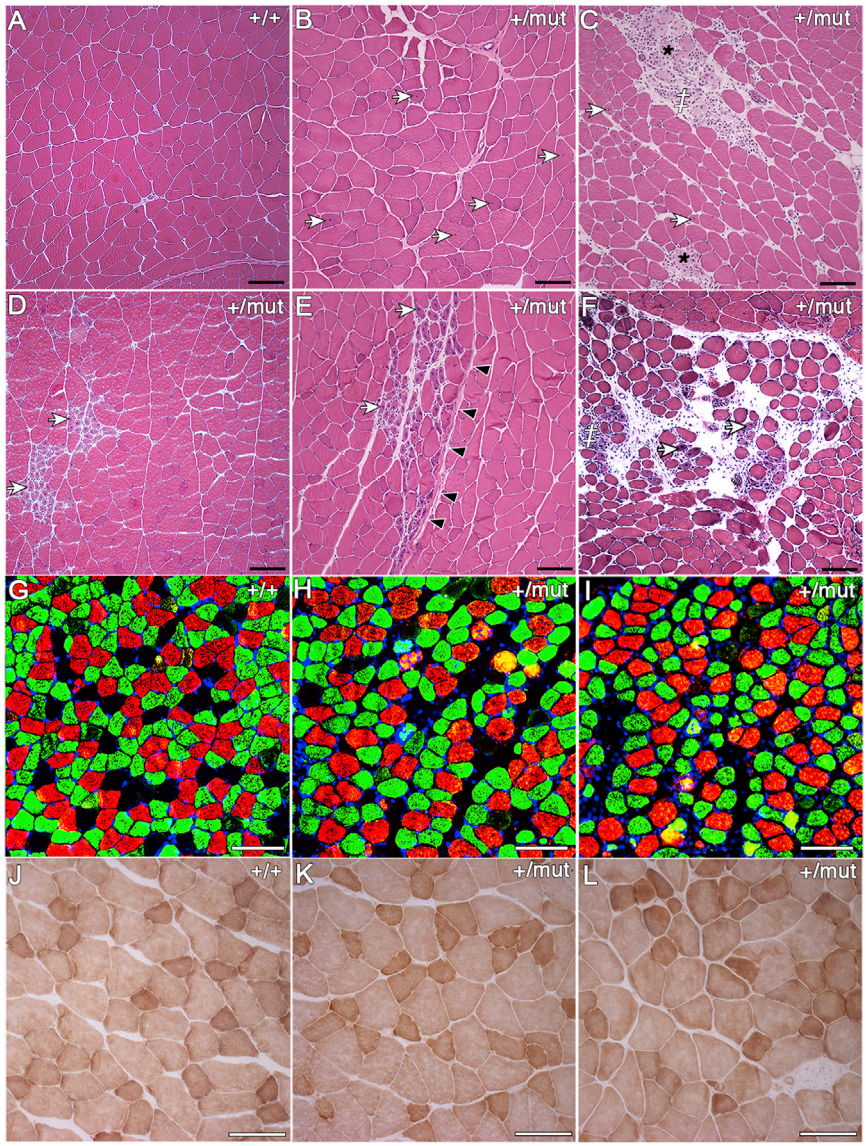

Figure 2. Myopathic Changes in Skeletal Muscles from *Col4a1* Mutant Mice Model the Human Disease

(A–F) H&E-stained sections of *Col4a1*$^{+/+}$ (A) and *Col4a1*$^{+/mut}$ (B–F) mouse quadriceps show a spectrum of focal histopathologic changes, including myofibers with NPN (white arrows in B–F); clusters of necrotic myofibers (* in C); endomysial and perifascicular clusters of regenerating myofibers containing NPN (D and E, respectively, black arrowheads in E demarcate the fascicle); infiltrating inflammatory cells (‡, C and F); and endomysial fibrosis (F).

(G–I) Dual MHC immunolabeling revealed normal distributions of type I (red) and type II (green) fibers in *Col4a1*-mutant skeletal muscles and a higher number of hybrid-type regenerating myofibers (yellow) in *Col4a1*-mutant skeletal muscles. (Compare mutant muscles [H and I] to wild-type muscle [G]).

(J–L) Histochemical staining for COX activity revealed no evidence of mitochondrial abnormalities in mutant muscles (K, unaffected area and L, lesion area) compared to control (J). Because the same spectrum of myopathic lesions was observed in *Col4a1*$^{+/G394V}$ and *Col4a1*$^{+/\Delta ex41}$ mice, images from *Col4a1*-mutant muscles were labeled as *Col4a1*$^{+/mut}$.

Scale barsrepresent 100 μm (A–I); and 50 μm (J–L).

Next, we crossed *Col4a1*$^{+/Flex41}$ mice to the *Tek*-Cre line to selectively express mutant COL4A1 in vascular endothelial cells. Mice that conditionally expressed mutant COL4A1 in vascular endothelium showed more NPN than did control mice (*Col4a1*$^{+/Flex41}$ and *Tek*^{Cre}). Moreover, the number of NPN in homozygous conditional mutant mice (*Tek*^{Cre}; *Col4a1*$^{Flex41/Flex41}$) was higher than in heterozygous conditional mutant mice (*Tek*^{Cre};*Col4a1*$^{+/Flex41}$) (Figures 6A–6C), and homozygous-conditional mutant mice had reduced grip strength (Figure 6D). To test whether a primary vascular insult might also contribute to peripheral hypomyelination, we evaluated MBP levels in sciatic nerves from P7 mice that conditionally express mutant COL4A1 in vascular endothelial cells, and we found that *Tek*^{Cre}; *Col4a1*$^{Flex41/Flex41}$ mice had slightly reduced MBP levels that did not reach statistical significance (Figures 6E and 6F). Together, these results conclusively establish that vascular defects contribute to myopathy in *Col4a1* mutant mice.

Differential Mutation-Specific Responses Suggest That the Presence of Mutant [α1(IV)]$_2$α2(IV) in the BM Can Contribute to Pathology

The pathogenicity of *COL4A1* mutations is generally attributed to impaired secretion of mutant [α1(IV)]$_2$α2(IV), and we previously showed that pharmacologically promoting [α1(IV)]$_2$α2(IV) secretion using 4PBA reduced ICHs and myopathy in *Col4a1*$^{+/\Delta ex41}$ mice.[15,16] To build on our recent findings and determine whether promoting [α1(IV)]$_2$α2(IV) secretion could provide long-term and general protective effects for COL4A1-related myopathy, we provided *Col4a1*$^{+/\Delta ex41}$ and *Col4a1*$^{+/G394V}$ mice with 4PBA from E9.5 to the age of 2 or 8 months, when we quantified NPN and grip strength. Although 4PBA had no effect on *Col4a1*$^{+/+}$ mice, it significantly reduced NPN numbers and improved grip strength in *Col4a1*$^{+/\Delta ex41}$ mice at both 2 and 8 months of age (Figures 7A–7D and Figures S4A–S4D, respectively). In striking contrast, 4PBA treatment led to an increase in NPN numbers in all muscle groups examined in *Col4a1*$^{+/G394V}$ mice, although there was no effect on grip force (Figures 7E–7K). These data support a model whereby the presence of mutant proteins in BMs can be pathogenic. Collectively, these findings identify a contrasting response to a potential

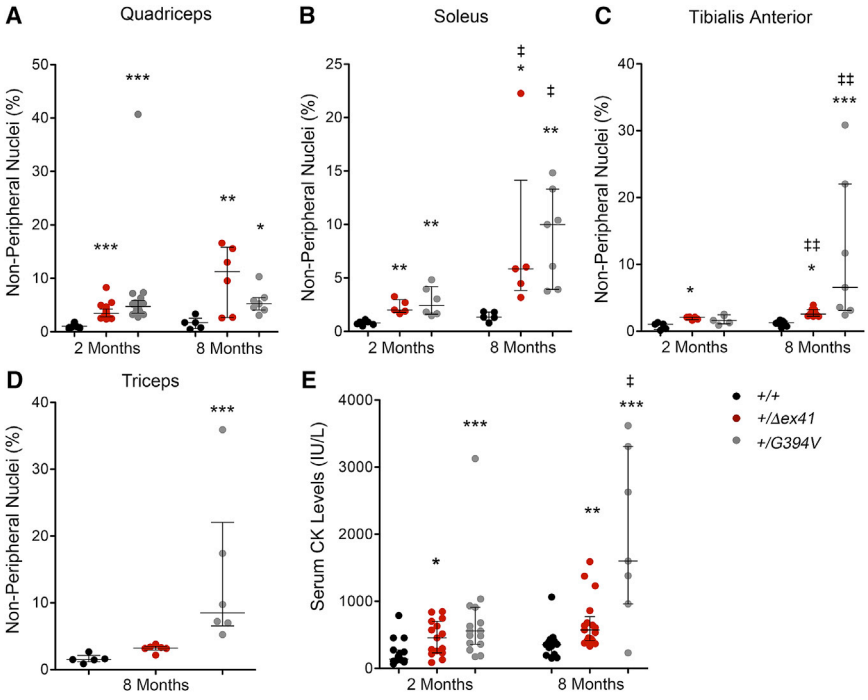

Figure 3. *Col4a1*- Mutant Mice Exhibit General and Progressive Skeletal Myopathy Characterized by Increased NPN Numbers and Serum CK Concentrations

(A–D) *Col4a1* mutant mice exhibit significantly increased NPN numbers in hindlimb (A–C) and forelimb (D) muscles and elevated serum CK concentrations (E) as compared to those of $Col4a1^{+/+}$ littermates.

Kruskal-Wallis tests with Dunnett pairwise tests (Bonferroni corrected): *$p < 0.05$; **$p < 0.01$; and ***$p < 0.001$). Comparison of NPN numbers and serum CK concentrations between the 2- and 8-month-old cohorts suggests that myopathy is progressive (Wilcoxon rank sum tests: ‡$p < 0.05$ and ‡‡$p < 0.01$). Data are presented as the median and interquartile range.

therapeutic strategy whereby pharmacological promotion of $[\alpha1(IV)]_2\alpha2(IV)$ secretion can ameliorate or exacerbate a particular phenotype in a mutation-dependent manner.

Dichotomous Intra-Allelic Responses to a Chemical Chaperone Reveal Tissue-Specific Mechanistic Heterogeneity

In addition to reducing ICH and myopathy severities in $Col4a1^{+/\Delta ex41}$ mice, 4PBA prevented peripheral nerve hypomyelination, as illustrated by increased MBP levels in P7 sciatic nerves (Figures 8A and 8C). To test whether the exacerbation of myopathy observed in 4PBA-treated $Col4a1^{+/G394V}$ mice resulted from an inherent property of this mutation that extends to other phenotypes, we compared peripheral nerve myelination and ICH severity in $Col4a1^{+/G394V}$ mice with and without 4PBA treatment. Similar to what we observed in $Col4a1^{+/\Delta ex41}$ mice, $Col4a1^{+/G394V}$ mice had reduced sciatic nerve MBP levels that were normalized by 4PBA administration (Figures 8B–8C), and $Col4a1^{+/G394V}$ mice had nearly undetectable ICHs, which were not exacerbated by 4PBA treatment (Figure 8D–8F). Thus, pharmacologically promoting $[\alpha1(IV)]_2\alpha2(IV)$ secretion had beneficial effects for all pathologies tested in $Col4a1^{+/\Delta ex41}$ mice, but had contrasting and tissue-specific effects in $Col4a1^{+/G394V}$ mice (where it exacerbated myopathy but ameliorated peripheral neuropathy and had no effect on ICHs).

Discussion

Col4a1 and *Col4a2* mutant mice recapitulate the pathophysiological manifestations observed in individuals with *COL4A1* and *COL4A2* mutations. The novel neuromuscular phenotypes described here expand the clinical spectrum of the COL4A1/A2 syndrome and provide significant biological insight into the underlying pathogenesis. Using a combination of histological, biochemical, functional, and genetic approaches, we show that tissue-specific allelic and mechanistic heterogeneities contribute to the neuromuscular manifestations caused by *Col4a1* mutations. Together, these findings underscore the importance of the $[\alpha1(IV)]_2\alpha2(IV)$ network as a multifunctional signaling platform that can elicit independent differential tissue-specific responses; these findings have broad implications for understanding and treatment of the COL4A1/A2 syndrome.

Myopathy is not well characterized in individuals with *COL4A1* and *COL4A2* mutations; only a few studies report nonspecific and widespread myopathic changes in biopsies.[5,33] Here, we performed a histopathological analysis of skeletal muscle samples from an individual previously described as having a *de novo COL4A1* mutation, c.2317G>A (p.Gly773Arg),[28] and we identify myopathy presenting as scattered lesions characterized by the presence of fibers in varying stages of necrosis and regeneration, endomysial fibrosis, and focal fatty infiltration. The subject also had cataracts, hypertrophic cardiomyopathy, and ischemic cerebrovascular pathology;[28] although metabolic myopathy was initially suggested, we found no evidence for a significant role of mitochondrial defects in the underlying disease process.[28] Out of ~130 published *COL4A1* mutations, the p.Gly775Arg mutation was described in four independent reports.[1,28,34–36] The clinical presentation of seven affected individuals from four unrelated families described in these studies was highly variable (even within a family) and included ICH, white-matter abnormalities, cataracts, ocular dysgenesis, muscle cramps, and serum CK concentration elevations. We have previously demonstrated that genetic context and

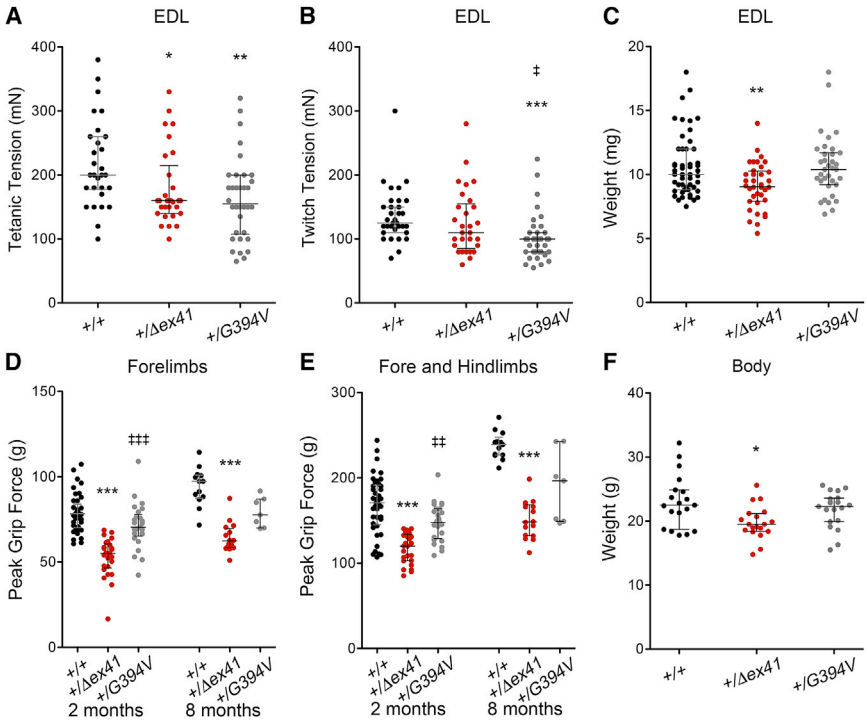

Figure 4. Deficits and Differences in Myomechanical Properties of *Col4a1* Mutant Mice

(A–C) Myomechanical analysis of isolated skeletal muscles demonstrates reduced force in *Col4a1*-mutant mice. Tetanic and twitch tensions were evaluated in extensor digitorum longus (EDL) muscles harvested from 2- 3-month-old $Col4a1^{+/+}$ and $Col4a1^{+/mut}$ mice (A and B). $Col4a1^{+/G394V}$ and $Col4a1^{+/\Delta ex41}$ mice exhibit significantly reduced maximal tetanic tension in comparison to $Col4a1^{+/+}$ littermates (A), and $Col4a1^{+/G394V}$ mice exhibit significant reduction in maximal twitch tension compared to $Col4a1^{+/+}$ and $Col4a1^{+/\Delta ex41}$ mice (B), suggesting more severe myopathy in $Col4a1^{+/G394V}$ mice than in $Col4a1^{+/\Delta ex41}$ mice. The EDL weight of 2-month-old $Col4a1^{+/\Delta ex41}$ mice but not of $Col4a1^{+/G394V}$ mice was reduced in comparison to that of $Col4a1^{+/+}$ mice (C). (D–F) $Col4a1^{+/\Delta ex41}$ and $Col4a1^{+/G394V}$ mice both had reduced forelimb (D) and fore- and hindlimb (E) peak grip forces compared to those of $Col4a1^{+/+}$ littermates at 2 and 8 months of age, but this reduction only reached statistical significance for $Col4a1^{+/\Delta ex41}$ mice. (F) The body weight of 2-month-old $Col4a1^{+/\Delta ex41}$ but not of $Col4a1^{+/G394V}$ mice was reduced in comparison to that of $Col4a1^{+/+}$ mice.
Data are presented as the median and interquartile range. Kruskal-Wallis tests with Dunnett pairwise tests (Bonferroni corrected): *$p < 0.05$; **$p < 0.01$; and ***$p < 0.001$ for comparison with $Col4a1^{+/+}$ mice or ‡$p < 0.05$; ‡‡$p < 0.01$; and ‡‡‡$p < 0.001$ for comparison between $Col4a1^{+/G394V}$ and $Col4a1^{+/\Delta ex41}$ mice.

environmental interactions contribute to variable expressivity of *Col4a1* mutations in mice,[2,5,10,16,37] and these clinical observations underscore the variable expressivity of *COL4A1* mutations among individuals with the same amino acid change.

We previously showed that allelic heterogeneity modulates the penetrance and severity of COL4A1-related pathologies, including ICHs and myopathy.[4,16] The relative severity of myopathy in $Col4a1^{+/G394V}$ mice and its exacerbation after 4PBA treatment suggest that this mutation directly disrupts a subdomain important for skeletal muscle function and implies the existence of subclasses of mutations with disproportionate contributions to tissue-specific pathologies. Notably, a cluster of *COL4A1* mutations is reported in a subset of individuals from six families who have a clinical diagnosis of HANAC syndrome (hereditary angiopathy with nephropathy, aneurysms, and muscle cramps,[17,38–40] MIM: 611773) and who typically present with muscle pathology. Although muscle cramps and serum CK elevation are characteristic manifestations observed in individuals with HANAC syndrome, cerebrovascular disease is usually clinically silent.[17,38–40] The mutations ascribed to HANAC syndrome (p.Gly498Asp, p.Gly498Val, p.Gly510Arg, p.Gly519Arg, p.Gly525Leu, and p.Gly528Asp) are spread over 30 amino acids in an area of the triple-helical domain containing putative interaction sites for multiple ECM-associated proteins and cell-surface receptors. However, none of the affected amino acids occur in clearly defined consensus binding sites.[41] Thus, it remains unresolved whether HANAC syndrome represents a distinct clinical or mechanistic entity whereby mutations directly perturb important functional subdomains[42] or falls within the broad spectrum of the COL4A1/A2 syndrome. A possible ascertainment bias could contribute to apparent genotype-phenotype correlations whereby subtle phenotypes (elevated CK or albuminuria) become more likely to be detected in the absence of life-threatening cerebrovascular disease (as predicted for individuals with mutations nearer the amino terminus of the protein).

Genetic alterations leading to disruption of the molecular networks linking the BM and myofiber cytoskeleton are well-established causes of congenital muscular dystrophies that often involve peripheral neuropathy.[43] Deficiency of the BM protein, laminin alpha 2 (LAMA2), or its cell-surface receptors, α7β1 integrin and the dystroglycan complex, cause congenital muscular dystrophy with peripheral neuropathy (MIM: 607855, 613204).[44–48] Although myopathy caused by *COL4A1* mutations is significantly milder than that observed in LAMA2-related myopathy, it is important to consider that *COL4A1* mutations are dominant and that LAMA2-related myopathy is typically only observed when homozygous or compound heterozygous mutations lead to near-complete absence of the protein. Furthermore, the biological importance of $[\alpha1(IV)]_2\alpha2(IV)$ in muscle homeostasis might be masked by co-morbidity

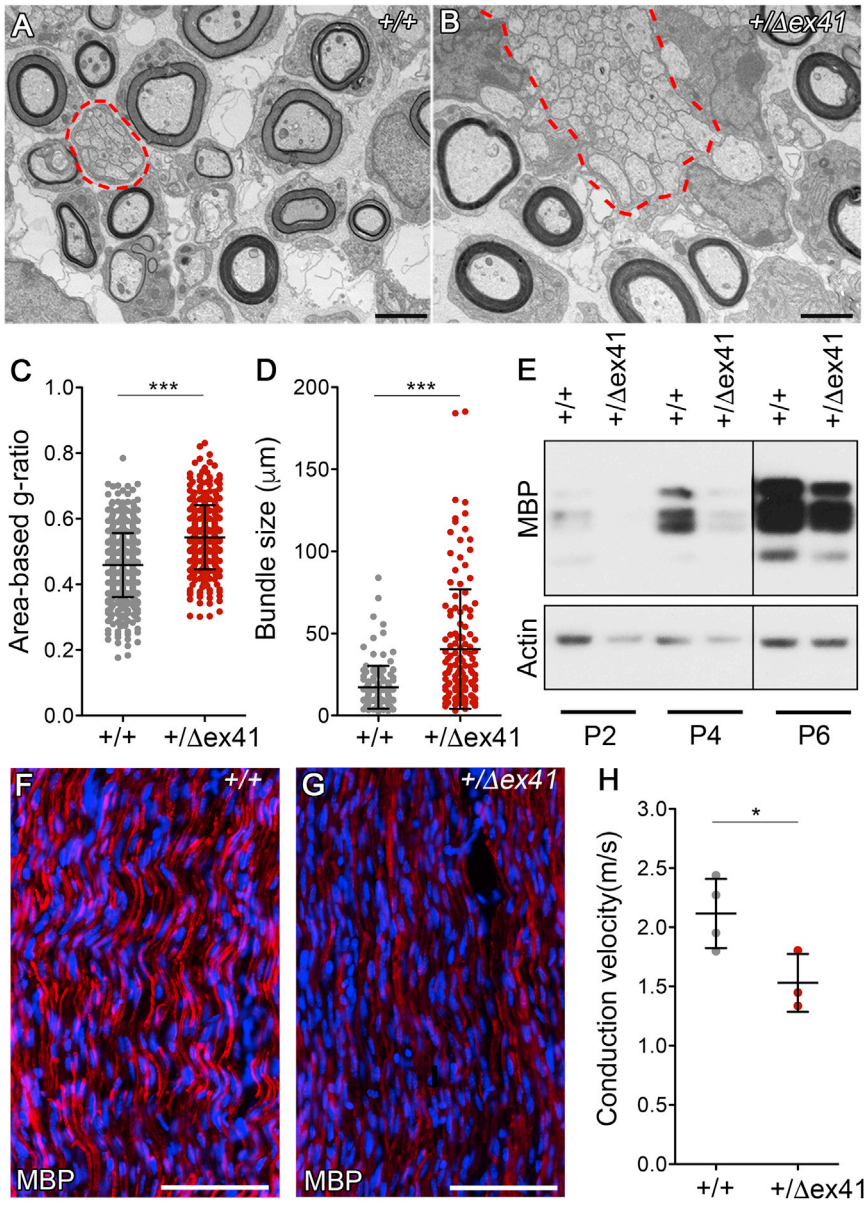

Figure 5. Peripheral Hypomyelination and Reduced Conduction Velocities in *Col4a1* Mutant Mice

(A–B) Representative micrographs of *Col4a1*$^{+/+}$ (A) and *Col4a1*$^{+/\Delta ex41}$ (B) sciatic nerves with unmyelinated axon bundles outlined with red dotted lines. Abnormally large bundles had irregular morphology, mixed-caliber axons, and an abnormally thin Schwann cell cytoplasm layer between individual axons, suggestive of impaired radial sorting.

(C) Quantification, using an area-based g-ratio, of myelin thickness from P6 sciatic nerves revealed hypomyelination in *Col4a1*$^{+/\Delta ex41}$ mice (n > 350 axons/genotype).

(D) Abnormally large bundles of unmyelinated axons were observed in P6 *Col4a1*$^{+/\Delta ex41}$ mice. Ultrastructural analyses were performed on 30 and 32 micrographs from six control and four mutant nerves, respectively.

(E) Representative immunoblot images showing reduced MBP amounts in sciatic nerves from *Col4a1*$^{+/\Delta ex41}$ mice compared to *Col4a1*$^{+/+}$ littermates at P2, P4, and P6.

(F–G) Representative images of P7 sciatic-nerve sections immunolabeled for MBP (MBP: red and DAPI: blue) showed reduced labeling in *Col4a1*$^{+/\Delta ex41}$ mice (G) compared to *Col4a1*$^{+/+}$ littermates (F).

(H) Conductance velocity was reduced in P7 sciatic nerves from *Col4a1*$^{+/\Delta ex41}$ mice compared to *Col4a1*$^{+/+}$ littermates.

Data are presented as the mean ± SD in (C) and (H) and as the median and interquartile range in (D). *p < 0.05; ***p < 0.001, by Student's t test (C and H) and Mann-Whitney test (D). Scale bars represent 2 μm (A and B) and 100 μm (F and G).

with other serious or fatal pathologies. The proximity of the *Col4a1*^{G394V} mutation to a putative integrin binding site (GFOGERGEK**G/V**) makes it tempting to speculate that this mutation locally disrupts the triple helix and impairs integrin binding.[41] However, *Col4a1*^{G394V} is adjacent to a consensus integrin α1β1/α2β1 binding motif, and α7β1 is the predominant integrin expressed by muscle fibers.[49–51] Regardless of the function of the putative integrin-binding domain, elucidating the molecular mechanisms underlying COL4A1-related neuromyopathy might also have therapeutic implications for individuals with *LAMA2* (MIM: 156225) mutations. For example, augmenting LAMA2-mediated linkages might ameliorate myopathy resulting from *COL4A1* and *COL4A2* mutations; reciprocally, the molecular pathways underlying COL4A1-related myopathy could represent alternative therapeutic targets for individuals with *LAMA2* mutations.

Identification of peripheral nerve hypomyelination in *Col4a1* mutant mice further reinforces the similarities between neuromuscular pathology caused by *COL4A1* and *LAMA2* mutations. In this case, COL4A1 and LAMA2 are extracellular ligands for the same adhesion G-protein-coupled receptor, GPR126, which is required for Schwann cell maturation and peripheral myelination.[29–31,52] The COL4A1 globular NC1 domain mediates the GPR126 interaction, which is consistent with mechanistically distinct functions for COL4A1 in skeletal muscles and peripheral nerves. Interestingly, type III collagen is an extracellular ligand for GPR56,[53] and perturbations cause cortical lamination defects that can also occur in the spectrum of phenotypes included in COL4A1/A2 syndrome.[5] Thus, it is possible that the COL4A1/A2 syndrome includes other aspects (including ocular dysgenesis, lamination defects, and white-matter abnormalities) that could be attributable to roles for COL4A1 and COL4A2 as ligands for diverse GPCRs. These observations support the idea that different

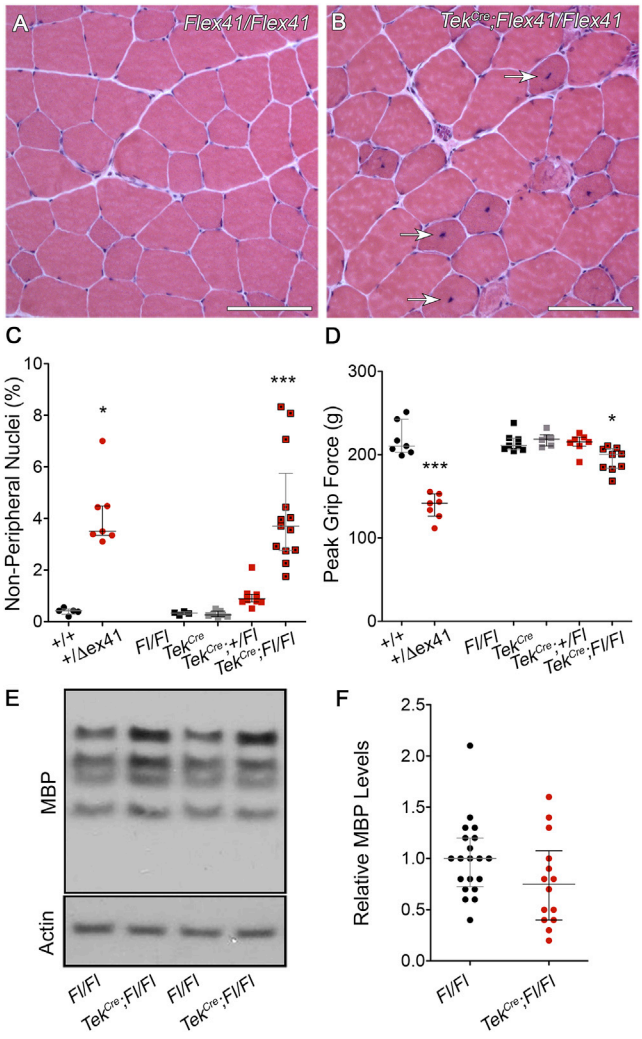

Figure 6. Vascular Contribution to the COL4A1-Related Neuromuscular Phenotype

(A and B) H&E-stained quadriceps sections from 3-month-old *Col4a1*$^{Flex41/\ Flex41}$ and *Tek*^{Cre}; *Col4a1*$^{Flex41/Flex41}$ mice show increased numbers of NPN (arrows) in *Tek*^{Cre};*Col4a1*$^{Flex41/Flex41}$ muscles.

(C) Control mice (*Tek*^{Cre} and *Col4a1*$^{Flex41/\ Flex41}$[Fl/Fl]) have NPN numbers that were indistinguishable from those of *Col4a1*$^{+/+}$ mice, and we observed a dose-dependent increase in NPN in *Tek*^{Cre};*Col4a1*$^{+/Flex41}$ and *Tek*^{Cre};*Col4a1*$^{Flex41/Flex41}$ mice.

(D) Similarly, *Tek*^{Cre};*Col4a1*$^{Flex41/Flex41}$, but not *Tek*^{Cre};*Col4a1*$^{+/Flex41}$, mice had reduced grip force.

(E–F) Immunoblot analysis suggests that MBP levels are mildly reduced in sciatic nerves from *Tek*^{Cre};*Col4a1*$^{Flex41/Flex41}$ compared to *Col4a1*$^{Flex41/\ Flex41}$ mice at P7.

Data are presented as the median and interquartile range. Kruskal-Wallis tests with Dunnett pairwise tests (Bonferroni corrected): *$p < 0.05$ and ***$p < 0.001$. The scale bar represents 100 μm.

COL4A1 functional subdomains mediate tissue-specific functions and are consistent with mechanistic heterogeneity in COL4A1-related myopathy and peripheral neuropathy.

A primary vascular etiology for COL4A1-related skeletal myopathy was suggested previously on the basis of muscle histopathology in *Col4a1*^{G498V} mutant mice, where ER stress was detected in vascular endothelial cells.[6] However, it remains to be determined whether ER stress is indeed causative and whether myopathy in *Col4a1*^{G498V}-mutant mice (a model for HANAC) primarily results from an intracellular vascular endothelial insult, as proposed,[6] or from an extracellular insult similar to that resulting from the *Col4a1*^{G394V} mutation presented here. Thus, determining whether myopathy is exacerbated or ameliorated in *Col4a1*$^{+/G498V}$ mice in response to 4PBA will be important for understanding whether HANAC is clinically and mechanistically distinct or simply part of the broad clinical spectrum of the general COL4A1/A2 syndrome. Regardless, selective expression of mutant COL4A1$^{\Delta ex41}$ in vascular endothelial cells mimics many aspects of the disease caused by ubiquitous expression of the mutant protein, clearly demonstrating that there is a vascular contribution to COL4A1-related myopathy. Furthermore, the discordant consequences of the *Col4a1*^{G394V} mutation on the severity of ICHs and myopathy and the contrasting tissue-specific responses to 4PBA treatment suggest that the molecular mechanisms underlying vascular and skeletal muscle pathologies are distinct. Collectively, the findings presented in this study suggest that independent and integrated muscular, neural, and vascular insults contribute to the overall neuromuscular phenotype caused by *Col4a1* mutations but that the underlying molecular mechanisms differ between tissues.

Together with our previous findings from an allelic series of *Col4a1* and *Col4a2* mutant mice, the current study offers a general model to explain the pathogenicity of *COL4A1* and *COL4A2* mutations; in this model the proximal insult for most mutations is a dominant-negative impairment of $[\alpha1(IV)]_2\alpha2(IV)$ secretion that functions as a graded series of hypomorphs for which the severity depends on their positions along the protein's amino-carboxy axis. ICHs appear to be a representative phenotype for this model and, as predicted, promoting $[\alpha1(IV)]_2\alpha2(IV)$ secretion suppresses ICHs.[15,16] Given that the GPR126 interaction is mediated by the NC1 domain, and in light of our current findings, we predict that peripheral nerve hypomyelination will follow the same genotype-phenotype profile followed by ICH severity. While the mechanism(s) underlying vascular pathology remain(s) unknown, the pathogenesis of peripheral neuropathy almost certainly involves extracellular deficiency rather than toxic cell-intrinsic accumulation of misfolded $[\alpha1(IV)]_2\alpha2(IV)$ in Schwann cell precursors. In contrast, the exacerbation of myopathy in *Col4a1*$^{+/G394V}$ mice treated with 4PBA indicates a qualitative, not quantitative, extracellular insult. Thus, neuromyopathy in *Col4a1* mutant mice appears to integrate at least three distinct pathogenic mechanisms in three different tissues.

The multi-functionality of the type IV collagen network presents a conceptual challenge for classifying mutations. Because COL4A1 has diverse extracellular roles, the qualitative or quantitative properties of a given mutation can vary in a tissue-specific manner. Thus, a specific mutation

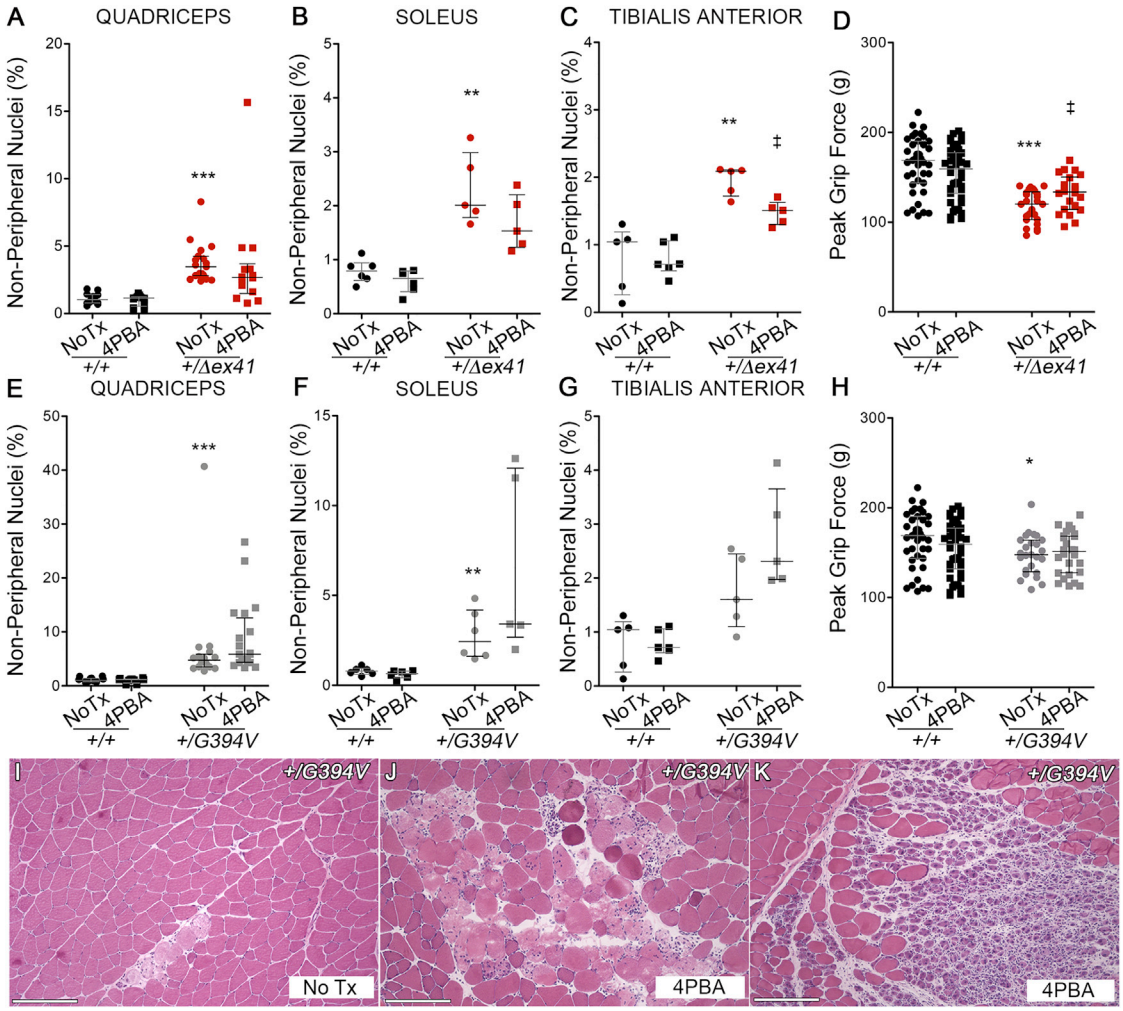

Figure 7. Mutation-Dependent Effect of 4PBA on COL4A1-Related Myopathy

(A–D) 4PBA treatment ameliorates myopathy in *Col4a1*$^{+/\Delta ex41}$ mice as shown by a reduction in the number of NPN in all muscles examined (A–C) and increased grip force (D) compared to untreated *Col4a1*$^{+/\Delta ex41}$ mice (no Tx) at 2 months of age.

(E–H) 4PBA treatment exacerbated myopathy in *Col4a1*$^{+/G394V}$ mice as shown by elevation in the number of NPN in all muscles examined; no effect on grip force was observed. The datasets for untreated and 4PBA-treated *Col4a1*$^{+/+}$ mice are duplicated to facilitate comparisons of NPN numbers and grip strength between *Col4a1*$^{+/+}$ and each *Col4a1* mutation.

Data are presented as median and interquartile ranges. Wilcoxon rank sum tests for comparisons between *Col4a1*$^{+/+}$ and *Col4a1*$^{+/Mut}$ strains (*$p < 0.05$; **$p < 0.01$; ***$p < 0.001$) and for testing the effect of 4PBA treatment for a given genotype ($^{‡}p < 0.05$). The scale bar represents 50 μM.

can simultaneously have cell-autonomous dominant-negative effects on $[\alpha1(IV)]_2\alpha2(IV)$ secretion and also have quantitative loss-of-function effects in one tissue and qualitative gain-of-function effects in another; these effects could be cell autonomous or non-autonomous. The dichotomous behavior of the *Col4a1*^{G394V} mutation across different tissues is a proof of concept for this important paradigm, and the classification of *COL4A1* and *COL4A2* mutations might become increasingly multi-dimensional as additional biological roles for $[\alpha1(IV)]_2\alpha2(IV)$ are identified. Given that mutations nearer the NC1 domain tend to cause more severe $[\alpha1(IV)]_2\alpha2(IV)$ secretion impairments, there might be an ascertainment bias toward identification of functional subdomains that are closer to the amino-terminal end of the protein in heterotrimers that reach the BM. Similarly, mutations with potential extracellular qualitative effects that occur near the NC1 domain might be "invisible" without artificially enhancing secretion of the mutant $[\alpha1(IV)]_2\alpha2(IV)$. Evaluating tissue-specific responses to 4PBA treatment across multiple mutations could be a useful tool for the mechanistic classification of mutations. Therapeutically promoting $[\alpha1(IV)]_2\alpha2(IV)$ secretion might end up being beneficial for the majority of mutations; however, this approach could exacerbate or induce tissue-specific pathologies for mutations occurring in specific functional subdomains. We predict that the eventual construction of a high-resolution map of functional subdomains for the type IV collagen network will guide the genetic stratification of human subjects into clinical and mechanistic subgroups that will distinguish those who are likely to benefit from promoting secretion from those

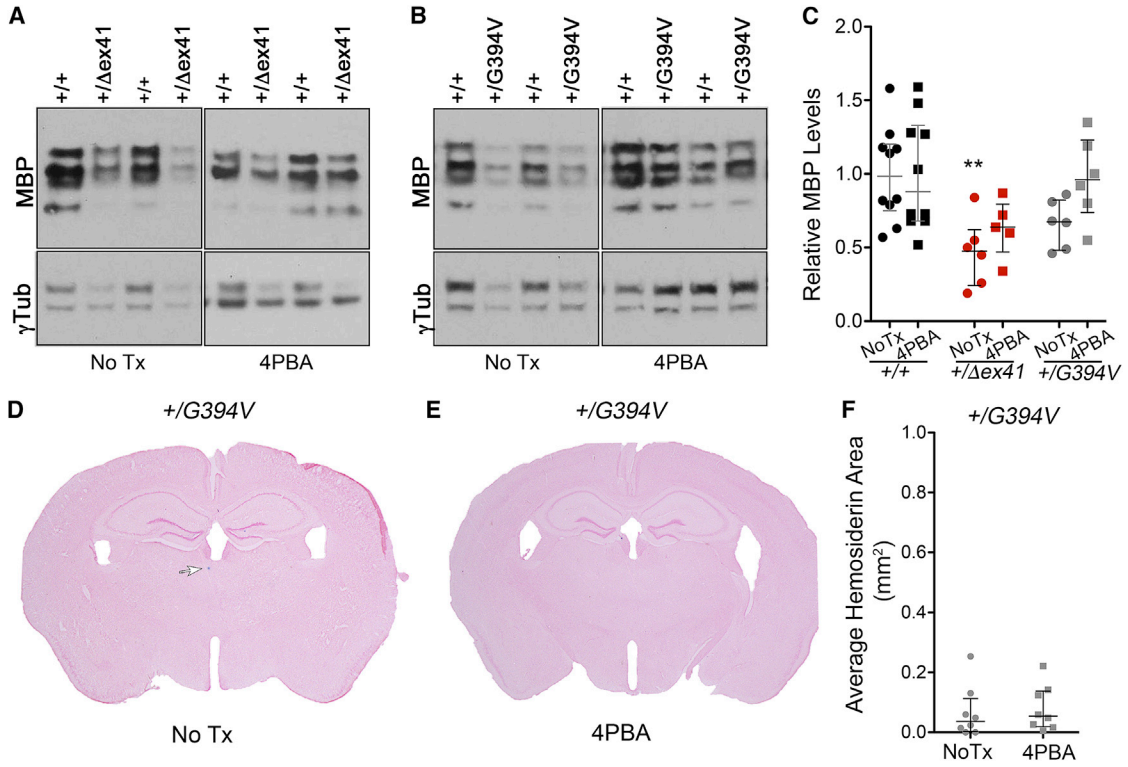

Figure 8. Tissue-Specific Response to 4PB4 Treatment in *Col4a1* Mutant Mice
(A–C) Representative immunoblots showing reduced MBP levels in P7 sciatic nerves from *Col4a1*$^{+/\Delta ex41}$ (A) and *Col4a1*$^{+/G394V}$ (B) mice compared to their respective *Col4a1*$^{+/+}$ littermates. 4PBA ameliorates myelination defects in both *Col4a1*$^{+/\Delta ex41}$ (A) and *Col4a1*$^{+/G394V}$ (B) mice. (Compare the relative difference in MBP amounts between untreated [no Tx] and 4PBA-treated *Col4a1*$^{+/+}$ and *Col4a1*$^{+/mut}$ littermates; this difference is quantified in [C]). γ-Tubulin was used as a loading control.
(D–F) Representative images of Prussian-blue-stained brain sections from untreated (no Tx) (D) and 4PBA-treated *Col4a1*$^{+/G394V}$ mice (E) and quantification of brain area covered by hemosiderin (F), showing no effect of 4PBA on ICH severity in *Col4a1*$^{+/G394V}$ mice.
Data are presented as the median and interquartile range. For comparisons between *Col4a1*$^{+/+}$ and *Col4a1*$^{+/mut}$ strains, p values were calculated via Kruskal-Wallis tests and Dunnett pairwise tests (Bonferroni corrected, **$p < 0.01$. Effect of 4PBA treatment for a given genotype was evaluated with Wilcoxon rank-sum tests.

who might require additional or alternative interventions that target distal extracellular insults. Finally, rather than assigning pathognomonic acronyms to clinical features, we propose a nosological classification of the COL4A1/A2 syndrome into clinically and mechanistically related disease subtypes as described for osteogenesis imperfecta (MIM: 166200, 166210, 259420, 166200, 613982) caused by mutations in *COL1A1* (MIM: 120150) and *COL1A2* (MIM: 120160) (e.g., COL4A1/A2 syndrome type I, type II, type III, etc.).

Supplemental Data

Supplemental Data can be found online at https://doi.org/10.1016/j.ajhg.2019.03.007.

Author Contributions

Conceived and designed the experiments: D.B.G. and C.L.D. Performed the experiments: C.L.D., V.S., G.H., K.H., D.Q.D., and G.W. Data analysis: C.L.D., G.H., D.Q.D., M.M., P.O., and D.B.G. Contributed reagents, materials, and/or analysis tools: M.M., P.O., E.M.U., and D.B.G. Writing of the manuscript: C.L.D. and D.B.G.

Acknowledgments

This work was supported by the National Institutes of Health (NS83830 to D.B.G., EY007120 to D.Q.D., and HL140942 to G.H.), Muscular Dystrophy Association (MDA295085 to D.B.G.), and American Heart Association (17POST33660668 to G.H.). The UCSF Department of Ophthalmology is supported by a core grant from the National Eye Institute (EY02162) and an unrestricted grant from Research to Prevent Blindness. Biostatistics consultation with Nancy Hills was funded by the National Center for Advancing Translational Sciences (UL1 TR001872). The BA-F8 and SC-71 monoclonal antibodies were developed by Schiaffino (University of Padova) and obtained from the Developmental Studies Hybridoma Bank, created by the NICHD of the NIH and maintained at the University of Iowa, Department of Biology, Iowa City, IA 52242.We thank Jonah Chan, Kelly Monk, and Stephen Fancy, as well as Yun-An Shen for helpful discussion and guidance with the sciatic nerve-related studies and Ivy Hsieh for assistance with electron microscopy.

Declaration of Interests

M.M. serves as a neuromuscular pathology consultant for Audentes Therapeutics. All other authors declare no competing interests.

Received: October 25, 2018
Accepted: March 5, 2019
Published: April 25, 2019

Web Resources

OMIM, https://www.omim.org

References

1. Jeanne, M., and Gould, D.B. (2017). Genotype-phenotype correlations in pathology caused by collagen type IV alpha 1 and 2 mutations. Matrix Biol. *57-58*, 29–44.
2. Mao, M., Alavi, M.V., Labelle-Dumais, C., and Gould, D.B. (2015). Type IV collagens and basement membrane diseases: cell biology and pathogenic mechanisms. Curr. Top. Membr. *76*, 61–116.
3. Kuo, D.S., Labelle-Dumais, C., and Gould, D.B. (2012). COL4A1 and COL4A2 mutations and disease: Insights into pathogenic mechanisms and potential therapeutic targets. Hum. Mol. Genet. *21* (R1), R97–R110.
4. Kuo, D.S., Labelle-Dumais, C., Mao, M., Jeanne, M., Kauffman, W.B., Allen, J., Favor, J., and Gould, D.B. (2014). Allelic heterogeneity contributes to variability in ocular dysgenesis, myopathy and brain malformations caused by Col4a1 and Col4a2 mutations. Hum. Mol. Genet. *23*, 1709–1722.
5. Labelle-Dumais, C., Dilworth, D.J., Harrington, E.P., de Leau, M., Lyons, D., Kabaeva, Z., Manzini, M.C., Dobyns, W.B., Walsh, C.A., Michele, D.E., and Gould, D.B. (2011). COL4A1 mutations cause ocular dysgenesis, neuronal localization defects, and myopathy in mice and Walker-Warburg syndrome in humans. PLoS Genet. *7*, e1002062.
6. Guiraud, S., Migeon, T., Ferry, A., Chen, Z., Ouchelouche, S., Verpont, M.C., Sado, Y., Allamand, V., Ronco, P., and Plaisier, E. (2017). HANAC Col4a1 mutation in mice leads to skeletal muscle alterations due to a primary vascular defect. Am. J. Pathol. *187*, 505–516.
7. Kelemen-Valkony, I., Kiss, M., Csiha, J., Kiss, A., Bircher, U., Szidonya, J., Maróy, P., Juhász, G., Komonyi, O., Csiszár, K., and Mink, M. (2012). Drosophila basement membrane collagen col4a1 mutations cause severe myopathy. Matrix Biol. *31*, 29–37.
8. Gupta, M.C., Graham, P.L., and Kramer, J.M. (1997). Characterization of alpha1(IV) collagen mutations in Caenorhabditis elegans and the effects of alpha1 and alpha2(IV) mutations on type IV collagen distribution. J. Cell Biol. *137*, 1185–1196.
9. Sibley, M.H., Graham, P.L., von Mende, N., and Kramer, J.M. (1994). Mutations in the alpha 2(IV) basement membrane collagen gene of Caenorhabditis elegans produce phenotypes of differing severities. EMBO J. *13*, 3278–3285.
10. Gould, D.B., Phalan, F.C., van Mil, S.E., Sundberg, J.P., Vahedi, K., Massin, P., Bousser, M.G., Heutink, P., Miner, J.H., Tournier-Lasserve, E., and John, S.W. (2006). Role of COL4A1 in small-vessel disease and hemorrhagic stroke. N. Engl. J. Med. *354*, 1489–1496.
11. Gould, D.B., Phalan, F.C., Breedveld, G.J., van Mil, S.E., Smith, R.S., Schimenti, J.C., Aguglia, U., van der Knaap, M.S., Heutink, P., and John, S.W. (2005). Mutations in Col4a1 cause perinatal cerebral hemorrhage and porencephaly. Science *308*, 1167–1171.
12. Fox, M.A., Sanes, J.R., Borza, D.B., Eswarakumar, V.P., Fässler, R., Hudson, B.G., John, S.W., Ninomiya, Y., Pedchenko, V., Pfaff, S.L., et al. (2007). Distinct target-derived signals organize formation, maturation, and maintenance of motor nerve terminals. Cell *129*, 179–193.
13. Fidler, A.L., Darris, C.E., Chetyrkin, S.V., Pedchenko, V.K., Boudko, S.P., Brown, K.L., Gray Jerome, W., Hudson, J.K., Rokas, A., and Hudson, B.G. (2017). Collagen IV and basement membrane at the evolutionary dawn of metazoan tissues. eLife *6*, e24176.
14. Hynes, R.O. (2012). The evolution of metazoan extracellular matrix. J. Cell Biol. *196*, 671–679.
15. Hayashi, G., Labelle-Dumais, C., and Gould, D.B. (2018). Use of sodium 4-phenylbutyrate to define therapeutic parameters for reducing intracerebral hemorrhage and myopathy in *Col4a1* mutant mice. Dis. Model. Mech. *11*, dmm034157.
16. Jeanne, M., Jorgensen, J., and Gould, D.B. (2015). Molecular and genetic analyses of collagen type IV mutant mouse models of spontaneous intracerebral hemorrhage identify mechanisms for stroke prevention. Circulation *131*, 1555–1565.
17. Plaisier, E., Chen, Z., Gekeler, F., Benhassine, S., Dahan, K., Marro, B., Alamowitch, S., Paques, M., and Ronco, P. (2010). Novel COL4A1 mutations associated with HANAC syndrome: a role for the triple helical CB3[IV] domain. Am. J. Med. Genet. A. *152A*, 2550–2555.
18. Jeanne, M., Labelle-Dumais, C., Jorgensen, J., Kauffman, W.B., Mancini, G.M., Favor, J., Valant, V., Greenberg, S.M., Rosand, J., and Gould, D.B. (2012). COL4A2 mutations impair COL4A1 and COL4A2 secretion and cause hemorrhagic stroke. Am. J. Hum. Genet. *90*, 91–101.
19. Favor, J., Gloeckner, C.J., Janik, D., Klempt, M., Neuhäuser-Klaus, A., Pretsch, W., Schmahl, W., and Quintanilla-Fend, L. (2007). Type IV procollagen missense mutations associated with defects of the eye, vascular stability, the brain, kidney function and embryonic or postnatal viability in the mouse, Mus musculus: an extension of the Col4a1 allelic series and the identification of the first two Col4a2 mutant alleles. Genetics *175*, 725–736.
20. Alavi, M.V., Mao, M., Pawlikowski, B.T., Kvezereli, M., Duncan, J.L., Libby, R.T., John, S.W., and Gould, D.B. (2016). Col4a1 mutations cause progressive retinal neovascular defects and retinopathy. Sci. Rep. *6*, 18602.
21. Lewandoski, M., Meyers, E.N., and Martin, G.R. (1997). Analysis of Fgf8 gene function in vertebrate development. Cold Spring Harb. Symp. Quant. Biol. *62*, 159–168.
22. Kisanuki, Y.Y., Hammer, R.E., Miyazaki, J., Williams, S.C., Richardson, J.A., and Yanagisawa, M. (2001). Tie2-Cre transgenic mice: a new model for endothelial cell-lineage analysis in vivo. Dev. Biol. *230*, 230–242.
23. Oishi, P.E., Cholsiripunlert, S., Gong, W., Baker, A.J., and Bernstein, H.S. (2011). Myo-mechanical analysis of isolated skeletal muscle. J. Vis. Exp. (48), e2582.
24. Bernstein, H.S., Samad, T., Cholsiripunlert, S., Khalifian, S., Gong, W., Ritner, C., Aurigui, J., Ling, V., Wilschut, K.J., Bennett, S., et al. (2013). Stem cell antigen-1 in skeletal muscle function. PLoS Curr. *5*, ecurrents.md.411a8332-d61e22725e6937b97e6d0ef8.
25. Shen, Y.A., Chen, Y., Dao, D.Q., Mayoral, S.R., Wu, L., Meijer, D., Ullian, E.M., Chan, J.R., and Lu, Q.R. (2014). Phosphorylation of LKB1/Par-4 establishes Schwann cell polarity to initiate and control myelin extent. Nat. Commun. *5*, 4991.
26. Dubowitz, V., and Sewry, C.A. (2007). Muscle biopsy: A practical approach (Philadelphia: Saunders/Elsevier).

27. Bloemberg, D., and Quadrilatero, J. (2012). Rapid determination of myosin heavy chain expression in rat, mouse, and human skeletal muscle using multicolor immunofluorescence analysis. PLoS ONE *7*, e35273.
28. Slavotinek, A.M., Garcia, S.T., Chandratillake, G., Bardakjian, T., Ullah, E., Wu, D., Umeda, K., Lao, R., Tang, P.L., Wan, E., et al. (2015). Exome sequencing in 32 patients with anophthalmia/microphthalmia and developmental eye defects. Clin. Genet. *88*, 468–473.
29. Paavola, K.J., Sidik, H., Zuchero, J.B., Eckart, M., and Talbot, W.S. (2014). Type IV collagen is an activating ligand for the adhesion G protein-coupled receptor GPR126. Sci. Signal. *7*, ra76.
30. Monk, K.R., Oshima, K., Jörs, S., Heller, S., and Talbot, W.S. (2011). Gpr126 is essential for peripheral nerve development and myelination in mammals. Development *138*, 2673–2680.
31. Monk, K.R., Naylor, S.G., Glenn, T.D., Mercurio, S., Perlin, J.R., Dominguez, C., Moens, C.B., and Talbot, W.S. (2009). A G protein-coupled receptor is essential for Schwann cells to initiate myelination. Science *325*, 1402–1405.
32. Mao, M., Kiss, M., Ou, Y., and Gould, D.B. (2017). Genetic dissection of anterior segment dysgenesis caused by a *Col4a1* mutation in mouse. Dis. Model. Mech. *10*, 475–485.
33. Yoneda, Y., Haginoya, K., Kato, M., Osaka, H., Yokochi, K., Arai, H., Kakita, A., Yamamoto, T., Otsuki, Y., Shimizu, S., et al. (2013). Phenotypic spectrum of COL4A1 mutations: porencephaly to schizencephaly. Ann. Neurol. *73*, 48–57.
34. Colin, E., Sentilhes, L., Sarfati, A., Mine, M., Guichet, A., Ploton, C., Boussion, F., Delorme, B., Tournier-Lasserve, E., and Bonneau, D. (2014). Fetal intracerebral hemorrhage and cataract: think COL4A1. J. Perinatol. *34*, 75–77.
35. Deml, B., Reis, L.M., Maheshwari, M., Griffis, C., Bick, D., and Semina, E.V. (2014). Whole exome analysis identifies dominant COL4A1 mutations in patients with complex ocular phenotypes involving microphthalmia. Clin. Genet. *86*, 475–481.
36. Shah, S., Kumar, Y., McLean, B., Churchill, A., Stoodley, N., Rankin, J., Rizzu, P., van der Knaap, M., and Jardine, P. (2010). A dominantly inherited mutation in collagen IV A1 (COL4A1) causing childhood onset stroke without porencephaly. Eur. J. Paediatr. Neurol. *14*, 182–187.
37. Gould, D.B., Marchant, J.K., Savinova, O.V., Smith, R.S., and John, S.W. (2007). Col4a1 mutation causes endoplasmic reticulum stress and genetically modifiable ocular dysgenesis. Hum. Mol. Genet. *16*, 798–807.
38. Alamowitch, S., Plaisier, E., Favrole, P., Prost, C., Chen, Z., Van Agtmael, T., Marro, B., and Ronco, P. (2009). Cerebrovascular disease related to COL4A1 mutations in HANAC syndrome. Neurology *73*, 1873–1882.
39. Plaisier, E., Alamowitch, S., Gribouval, O., Mougenot, B., Gaudric, A., Antignac, C., Roullet, E., and Ronco, P. (2005). Autosomal-dominant familial hematuria with retinal arteriolar tortuosity and contractures: a novel syndrome. Kidney Int. *67*, 2354–2360.
40. Plaisier, E., Gribouval, O., Alamowitch, S., Mougenot, B., Prost, C., Verpont, M.C., Marro, B., Desmettre, T., Cohen, S.Y., Roullet, E., et al. (2007). COL4A1 mutations and hereditary angiopathy, nephropathy, aneurysms, and muscle cramps. N. Engl. J. Med. *357*, 2687–2695.
41. Parkin, J.D., San Antonio, J.D., Pedchenko, V., Hudson, B., Jensen, S.T., and Savige, J. (2011). Mapping structural landmarks, ligand binding sites, and missense mutations to the collagen IV heterotrimers predicts major functional domains, novel interactions, and variation in phenotypes in inherited diseases affecting basement membranes. Hum. Mutat. *32*, 127–143.
42. Chen, Z., Migeon, T., Verpont, M.C., Zaidan, M., Sado, Y., Kerjaschki, D., Ronco, P., and Plaisier, E. (2016). HANAC syndrome Col4a1 mutation causes neonate glomerular hyperpermeability and adult glomerulocystic kidney disease. J. Am. Soc. Nephrol. *27*, 1042–1054.
43. Carmignac, V., and Durbeej, M. (2012). Cell-matrix interactions in muscle disease. J. Pathol. *226*, 200–218.
44. Michele, D.E., Barresi, R., Kanagawa, M., Saito, F., Cohn, R.D., Satz, J.S., Dollar, J., Nishino, I., Kelley, R.I., Somer, H., et al. (2002). Post-translational disruption of dystroglycan-ligand interactions in congenital muscular dystrophies. Nature *418*, 417–422.
45. Cohn, R.D., Henry, M.D., Michele, D.E., Barresi, R., Saito, F., Moore, S.A., Flanagan, J.D., Skwarchuk, M.W., Robbins, M.E., Mendell, J.R., et al. (2002). Disruption of DAG1 in differentiated skeletal muscle reveals a role for dystroglycan in muscle regeneration. Cell *110*, 639–648.
46. Hayashi, Y.K., Chou, F.L., Engvall, E., Ogawa, M., Matsuda, C., Hirabayashi, S., Yokochi, K., Ziober, B.L., Kramer, R.H., Kaufman, S.J., et al. (1998). Mutations in the integrin alpha7 gene cause congenital myopathy. Nat. Genet. *19*, 94–97.
47. Mayer, U., Saher, G., Fässler, R., Bornemann, A., Echtermeyer, F., von der Mark, H., Miosge, N., Pöschl, E., and von der Mark, K. (1997). Absence of integrin alpha 7 causes a novel form of muscular dystrophy. Nat. Genet. *17*, 318–323.
48. Helbling-Leclerc, A., Zhang, X., Topaloglu, H., Cruaud, C., Tesson, F., Weissenbach, J., Tomé, F.M., Schwartz, K., Fardeau, M., Tryggvason, K., et al. (1995). Mutations in the laminin alpha 2-chain gene (LAMA2) cause merosin-deficient congenital muscular dystrophy. Nat. Genet. *11*, 216–218.
49. Leitinger, B., and Hohenester, E. (2007). Mammalian collagen receptors. Matrix Biol. *26*, 146–155.
50. White, D.J., Puranen, S., Johnson, M.S., and Heino, J. (2004). The collagen receptor subfamily of the integrins. Int. J. Biochem. Cell Biol. *36*, 1405–1410.
51. Vandenberg, P., Kern, A., Ries, A., Luckenbill-Edds, L., Mann, K., and Kühn, K. (1991). Characterization of a type IV collagen major cell binding site with affinity to the alpha 1 beta 1 and the alpha 2 beta 1 integrins. J. Cell Biol. *113*, 1475–1483.
52. Petersen, S.C., Luo, R., Liebscher, I., Giera, S., Jeong, S.J., Mogha, A., Ghidinelli, M., Feltri, M.L., Schöneberg, T., Piao, X., and Monk, K.R. (2015). The adhesion GPCR GPR126 has distinct, domain-dependent functions in Schwann cell development mediated by interaction with laminin-211. Neuron *85*, 755–769.
53. Luo, R., Jeong, S.J., Jin, Z., Strokes, N., Li, S., and Piao, X. (2011). G protein-coupled receptor 56 and collagen III, a receptor-ligand pair, regulates cortical development and lamination. Proc. Natl. Acad. Sci. USA *108*, 12925–12930.